Investigation of the Longitudinal Multiconductor Transmission Line Functions for Symmetric Coupled-Microstrip Systems

Josh G. Nickel, *Student Member, IEEE,* and José E. Schutt-Ainé, *Senior Member, IEEE*

***Abstract*—In inhomogeneous multiconductor transmission line (MTL) structures such as coupled microstrip, propagation is characterized by multiple quasi-TEM modes with distinct propagation constants. These "mode delays" cause the MTL functions to exhibit longitudinal behavior that superficially appears problematic in the context of passive lossless reciprocal systems. This paper presents a thorough investigation of the longitudinal MTL functions. Using MTL formulation and computer simulation, we explain the mathematics and physics of mode delays so that their effects are not misinterpreted or attributed to error in the numerical analysis of MTLs.**

***Index Terms*—Coupled microstrip, immittance matrices, modal dispersion, multiconductor transmission lines.**

I. Introduction

In INHOMOGENEOUS multiconductor transmission line (MTL) systems, the distinct propagation constants result in "mode delays" along the longitudinal direction. These systems have been termed "multivelocity transmission lines" [1]. The general well-known MTL conductor- and mode-domain formulations that consider mode delays [2]–[7] are widely applicable to many microwave problems with moderate to high coupling (e.g., crosstalk prediction). However, to the authors' knowledge, no comprehensive study of these MTL quantities as functions of longitudinal distance from a termination or discontinuity has been undertaken. One present motivation for such analysis is MTL matching network synthesis and transistor amplifier design [8].

This investigation will focus on the longitudinal behavior of the MTL functions, including the signals and longitudinal immittance matrix functions (LIMFs). Past work on MTL immittance matrices has concerned their derivation for fixed-length structures [9]–[11]. "Immittance" in this paper implies the impedance, admittance, reflection coefficient, or scattering matrix *looking into a terminated line of some specified length*. In particular, we will address several seemingly problematic effects of the mode delays on these longitudinal MTL functions. For example, consider that lossless reciprocal two-conductor transmission lines exhibit several intuitive longitudinal properties: positive resistive and conductive components of input impedances and admittances, and constant reflection coefficient magnitude. However, these properties *do not* generally apply to the matrix and vector elements of the longitudinal MTL functions in steady-state conditions. We will show how the longitudinal conductor admittance matrices (in a passive system) do not necessarily have negative off-diagonal real parts. Similar works have considered the signs of characteristic matrix terms in asymmetric lines [12].

In this paper, our principal goal is to investigate, explain, and validate these effects so they are not attributed to numerical errors or nonphysical behavior. First, the MTL equations are overviewed briefly. Next, the longitudinal properties of immittance matrices and signals in symmetric lossless reciprocal MTL systems are detailed (we limit this analysis to inhomogeneous symmetric systems and terminations) for arbitrary passive linear termination. The effects of mode delays on all MTL functions is detailed and relevant physical interpretations are drawn. Numerical results from simulation illustrate these effects.

II. MTL Equations

Consider a symmetric coupled microstrip structure with an arbitrary number of lines n and $N = n + 1$ conductors where the ground plane is reference. While we focus in this paper on the three-line $(n = 3)$ case, results are generalized to n lines where possible. The n-line MTL equations are equivalent to the telegrapher's equations in frequency-domain matrix form (sinusoidal steady-state conditions), and include the $(n \times n)$ symmetric complex matrices of per-unit-length impedance and admittance $\boldsymbol{Z}$ and $\boldsymbol{Y}$.

In n-line quasi-TEM analysis, the n propagating modes are interpreted as physical system voltages and currents [2]. Decoupled telegrapher's wave equations are solved via linear transformation for the conductor and mode variables

$$\boldsymbol{v}_m(z) = \boldsymbol{E} \cdot \boldsymbol{v}_c(z) \tag{1a}$$

$$\boldsymbol{i}_m(z) = \boldsymbol{H} \cdot \boldsymbol{i}_c(z) \tag{1b}$$

where $\boldsymbol{E}$ and $\boldsymbol{H}$ are $(n \times n)$ transformation matrices, which simultaneously diagonalize both $\boldsymbol{Z}$ and $\boldsymbol{Y}$ to uncouple the MTL equations. These transformations are redefined such that $\boldsymbol{E} \cdot \boldsymbol{H}^t = \boldsymbol{1}_n$ [7]. The n-column vectors $\boldsymbol{v}_m(z)$ and $\boldsymbol{i}_m(z)$ are the mode voltage and current vectors along the line. Vectors $\boldsymbol{v}_c(z)$ and $\boldsymbol{i}_c(z)$ are the $(n \times 1)$ conductor voltage and current vectors, respectively, with z being the longitudinal coordinate and $e^{j\omega t}$

Manuscript received February 4, 2000; revised November 16, 2000.

J. G. Nickel was with the Center for Computational Electromagnetics, Department of Electrical and Computer Engineering, University of Illinois at Urbana-Champaign, Urbana, IL 61801 USA. He is now with Silicon Bandwidth, Fremont, CA 94538 USA (e-mail: josh@hspark.ece.uiuc.edu).

J. E. Schutt-Ainé is with the Center for Computational Electromagnetics, Department of Electrical and Computer Engineering, University of Illinois at Urbana-Champaign, Urbana, IL 61801 USA (e-mail: jose@decwa.ece.uiuc.edu).

Publisher Item Identifier S 0018-9480(02)00739-1.

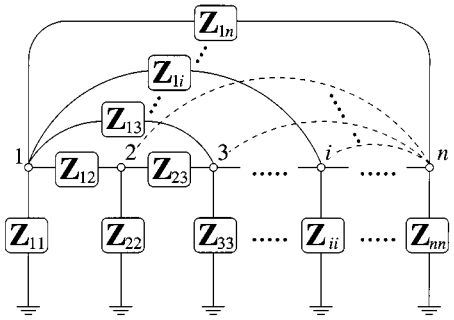

Fig. 1. n-port N-node common-ground impedance network matrix physical circuit realization for an $(n \times n)$ admittance matrix. Note: $\mathbf{Z}_{ij} = [\boldsymbol{\mathcal{Z}}_L]_{ij}$.

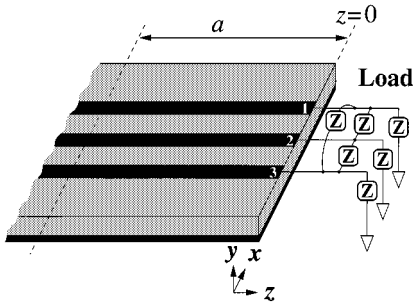

Fig. 2. Coupled transmission-line section with load terminations and immittance matrices at $z = -a$.

being suppressed. For microstrip, there are generally n distinct complex quasi-TEM mode propagation constants $\gamma_{i=1,2,\ldots,n}$ arranged in matrix $\boldsymbol{\Lambda}_m$.

Total mode voltage and current vectors are expressed as the superposition of forward and backward waves [7]

$$\boldsymbol{v}_m(z) = \boldsymbol{Q}(-z)\cdot\boldsymbol{v}_m^+ + \boldsymbol{Q}(z)\cdot\boldsymbol{v}_m^- \quad (2a)$$

$$\boldsymbol{i}_m(z) = \boldsymbol{Q}(-z)\cdot\boldsymbol{i}_m^+ - \boldsymbol{Q}(z)\cdot\boldsymbol{i}_m^- \quad (2b)$$

where $\boldsymbol{v}_m^{\pm}$ and $\boldsymbol{i}_m^{\pm}$ are the modal wave coefficient vectors at the load $(z = 0)$, and $\boldsymbol{Q}(z)$ is a diagonal matrix whose entries are $e^{\gamma_i z}$, with γ_i denoting the complex propagation constant of the ith mode.

Diagonal-mode characteristic impedance and admittance matrices are [13], [14]

$$\boldsymbol{Z}_{\rm ch}^m = \boldsymbol{\Lambda}_m^{-1}\cdot\boldsymbol{E}\cdot\boldsymbol{Z}\cdot\boldsymbol{H}^{-1} = \boldsymbol{E}\cdot\boldsymbol{Y}^{-1}\cdot\boldsymbol{H}^{-1}\cdot\boldsymbol{\Lambda}_m \quad (3a)$$

$$\boldsymbol{Y}_{\rm ch}^m = \boldsymbol{\Lambda}_m^{-1}\cdot\boldsymbol{H}\cdot\boldsymbol{Y}\cdot\boldsymbol{E}^{-1} = \boldsymbol{H}\cdot\boldsymbol{Z}^{-1}\cdot\boldsymbol{E}^{-1}\cdot\boldsymbol{\Lambda}_m \quad (3b)$$

while the conductor characteristic impedance and admittance matrices are easily derived from [13], [14]

$$\boldsymbol{Z}_{\rm ch}^c = \boldsymbol{E}^{-1}\cdot\boldsymbol{\Lambda}_m^{-1}\cdot\boldsymbol{E}\cdot\boldsymbol{Z} = \boldsymbol{Y}^{-1}\cdot\boldsymbol{H}^{-1}\boldsymbol{\Lambda}_m\cdot\boldsymbol{H} \quad (4a)$$

$$\boldsymbol{Y}_{\rm ch}^c = \boldsymbol{H}^{-1}\cdot\boldsymbol{\Lambda}_m^{-1}\cdot\boldsymbol{H}\cdot\boldsymbol{Y} = \boldsymbol{Z}^{-1}\cdot\boldsymbol{E}^{-1}\cdot\boldsymbol{\Lambda}_m\cdot\boldsymbol{E} \quad (4b)$$

where the superscript c denotes the *conductor*.

A. Terminated MTL Structure

Now suppose the coupled lines are terminated at one end with a passive linear circuit network comprised of impedances interconnecting each of the N conductors in a common-ground topology at the termination plane $z = 0$, as illustrated in Fig. 1. This is an "N-terminal" topology, i.e., one of the N nodes is designated the common ground to which all n ports are referenced. We conveniently express this termination in an $(n \times n)$ "impedance network matrix" $[\boldsymbol{\mathcal{Z}}_L]$. The diagonal term $[\boldsymbol{\mathcal{Z}}_L]_{ii}$ represents the impedance connecting line i to ground, and the off-diagonal term $[\boldsymbol{\mathcal{Z}}_L]_{ij}$ represents the impedance connecting lines i and j. The dual-admittance network matrix is the term-wise reciprocal of the impedance network matrix $[\boldsymbol{\mathcal{Y}}_L]_{ij} = ([\boldsymbol{\mathcal{Z}}_L]_{ij})^{-1}$. Note that these matrices have little mathematical meaning $\left([\boldsymbol{\mathcal{Y}}_L] \neq [\boldsymbol{\mathcal{Z}}_L]^{-1}\right)$, they are merely compact physical representations of networks; hence, the calligraphic denotation.

To analyze reflections on coupled lines, as in Fig. 2 (a specific three-line system considered in the numerical results), the termination networks must be expressed as $(n \times n)$ conductor open-circuit impedance or short-circuit admittance matrices. We denote these $\boldsymbol{Z}_L^c$ and $\boldsymbol{Y}_L^c$ $\left([\boldsymbol{Z}_L^c] = [\boldsymbol{Y}_L^c]^{-1}\right)$. Matrix $\boldsymbol{Y}_L^c$ is easily synthesized from $\boldsymbol{\mathcal{Y}}_L$ as follows:

$$[\boldsymbol{Y}_L^c]_{ii} = \sum_{k=1}^{n}([\boldsymbol{\mathcal{Z}}_L]_{ik})^{-1}, \qquad i = 1, 2, \ldots, n \quad (5a)$$

$$[\boldsymbol{Y}_L^c]_{ij} = (-[\boldsymbol{\mathcal{Z}}_L]_{ij})^{-1}, \qquad i \neq j. \quad (5b)$$

The mode or conductor reflection coefficient at the load that relates the mode or conductor voltage vectors $\boldsymbol{v}_{m,c}^+$ to $\boldsymbol{v}_{m,c}^-$ by $\boldsymbol{v}_{m,c}^- = \boldsymbol{\Gamma}_L^{m,c}\cdot\boldsymbol{v}_{m,c}^+$ is derived from boundary conditions [7], [8], [15], i.e., evaluating (1) and (2) at $z = 0$ as follows:

$$\boldsymbol{\Gamma}_L^{m,c} = [\boldsymbol{Z}_L^{m,c} - \boldsymbol{Z}_{\rm ch}^{m,c}]\cdot[\boldsymbol{Z}_L^{m,c} + \boldsymbol{Z}_{\rm ch}^{m,c}]^{-1} \quad (6a)$$

$$= [\boldsymbol{Y}_{\rm ch}^{m,c} + \boldsymbol{Y}_L^{m,c}]^{-1}\cdot[\boldsymbol{Y}_{\rm ch}^{m,c} - \boldsymbol{Y}_L^{m,c}]. \quad (6b)$$

Matrix $\boldsymbol{Y}_L^m$ is the mode admittance at the load

$$\boldsymbol{Y}_L^m = \boldsymbol{H}\cdot\boldsymbol{Y}_L^c\cdot\boldsymbol{E}^{-1} \quad (7)$$

which is generally not diagonal.

Both reflection coefficient matrices are asymmetric in general, even for symmetric lines and terminations, though this case leads to several simplifications. Matrix $\boldsymbol{\Gamma}_L^m$ contains $[n/2]$ zeros (where brackets denote integer part) for terms whose indexes are related by $(i-j) \bmod 2 = 1$ [15]. This is a consequence of the termination symmetry, where incident even modes do not excite reflected odd modes and vice-versa. Matrix $\boldsymbol{\Gamma}_L^c$ possesses some symmetry, namely,

$$[\boldsymbol{\Gamma}_L^c]_{i,j} = [\boldsymbol{\Gamma}_L^c]_{n-i+1,n-j+1}. \quad (8)$$

This property follows from the assumption that the n lines are symmetric about the $x = 0$-plane. The asymmetry will be addressed in Section II-C.

The conductor current reflection coefficient matrix is the transpose of the conductor voltage reflection coefficient matrix, as easily shown using power relations or through direct boundary condition derivation (we highlight that the result may differ in sign from [7], simply by convention). However, we consider only the conductor voltage reflection coefficient $\boldsymbol{\Gamma}_{\rm in}^c(z)$ for the remainder of this paper.

B. Longitudinal MTL Functions

Longitudinal MTL functions depend on the n quasi-TEM propagation constants. The mode reflection coefficient matrix looking toward the load (input) is

$$\boldsymbol{\Gamma}^m_{\rm in}(z) = \boldsymbol{Q}(z) \cdot \boldsymbol{\Gamma}^m_L \cdot \boldsymbol{Q}(z) \tag{9}$$

and the conductor reflection coefficient matrix is

$$\boldsymbol{\Gamma}^c_{\rm in}(z) = \boldsymbol{E}^{-1} \cdot \boldsymbol{\Gamma}^m_{\rm in}(z) \cdot \boldsymbol{E}. \tag{10}$$

At an arbitrary point $z = -a$, either matrix may be converted to an admittance matrix which, if realized, would terminate the lines at $z = -a$ with an N-terminal passive circuit, as in Fig. 1, and equivalently model the immittance parameters of the coupled-line section of length a between the observation point and the termination shown in Fig. 2.

The longitudinal impedance and admittance matrices are expressed [15]–[17] in modal and conductor form as

$$\boldsymbol{Z}^{m,c}_{\rm in}(z) = [\mathbf{1}_n - \boldsymbol{\Gamma}^{m,c}_{\rm in}(z)]^{-1} \cdot [\mathbf{1}_n + \boldsymbol{\Gamma}^{m,c}_{\rm in}(z)]\, \boldsymbol{Z}^{m,c}_{\rm ch} \tag{11}$$

$$\boldsymbol{Y}^{m,c}_{\rm in}(z) = \boldsymbol{Y}^{m,c}_{\rm ch}\, [\mathbf{1}_n + \boldsymbol{\Gamma}^{m,c}_{\rm in}(z)]^{-1} \cdot [\mathbf{1}_n - \boldsymbol{\Gamma}^{m,c}_{\rm in}(z)]. \tag{12}$$

Network matrices corresponding to these are (5)

$$[\boldsymbol{\mathcal{Z}}_{\rm in}(z)]_{ii} = \left(\sum_{k=1}^{n} [\boldsymbol{Y}^c_{\rm in}(z)]_{ik} \right)^{-1}, \qquad i = 1, 2, \ldots, n$$

$$[\boldsymbol{\mathcal{Z}}_{\rm in}(z)]_{ij} = \left(- [\boldsymbol{Y}^c_{\rm in}(z)]_{ij} \right)^{-1}, \qquad i \neq j \tag{13a}$$

$$[\boldsymbol{\mathcal{Y}}_{\rm in}(z)]_{ij} = ([\boldsymbol{\mathcal{Z}}_{\rm in}(z)]_{ij})^{-1}, \qquad \text{all } i, j. \tag{13b}$$

C. Asymmetry and Reciprocity in MTL Functions

One may easily show that $\boldsymbol{Z}^c_{\rm in}(z)$ and $\boldsymbol{Y}^c_{\rm in}(z)$ are symmetric in reciprocal systems. Despite the symmetry of the terms in (6a), these factors do not necessarily commute, resulting in general asymmetry of the reflection coefficient matrices. Physically, a voltage on line i incident upon a symmetric termination does not "see" the same circuit as an incident voltage on line j, hence, the reflected signal on line j due to the incident signal on line i does not relate in a simple manner to the reflected signal on line j due to the incident signal on line i.

However, this property has no bearing on reciprocity since it does not relate electromagnetic reactions. Instead, we must consider symmetry of the $(n \times n)$ input conductor S-parameter matrix $\boldsymbol{S}^c_{\rm in}(z)$ (referenced to impedance $\boldsymbol{Z}^c_{\rm ch}$), which relates the longitudinal power waves $\boldsymbol{a}^c(z)$ and $\boldsymbol{b}^c(z)$ by $\boldsymbol{b}^c_{\rm in}(z) = \boldsymbol{S}^c_{\rm in}(z) \cdot \boldsymbol{a}^c_{\rm in}(z)$. In general, $\boldsymbol{\Gamma}^c_{\rm in}(z)$ and $\boldsymbol{S}^c_{\rm in}(z)$ of the n-port at z are not equivalent (the exception being for diagonal $\boldsymbol{Z}^c_{\rm ch}$ with all diagonal terms equal). Matrix $\boldsymbol{S}^c_{\rm in}(z)$ is derived from (6) and the power wave normalizations

$$\boldsymbol{S}^c = (\boldsymbol{Z}^c_{\rm ch})^{1/2} \cdot [\boldsymbol{Z}^c_{\rm ch} + \boldsymbol{Z}^c_L]^{-1} \cdot [\boldsymbol{Z}^c_L - \boldsymbol{Z}^c_{\rm ch}] \cdot (\boldsymbol{Z}^c_{\rm ch})^{-1/2}. \tag{14}$$

By reciprocity, an excitation of a_1 on port 1 is scaled by S_{21} to produce b_2 on port 2; an excitation of a_2 on port 2 is scaled by S_{12} to produce b_1 on port 1. Even for dense $\boldsymbol{Z}^c_{\rm ch}$, $\boldsymbol{S}$ is symmetric and, therefore, reciprocal (see Appendix).

III. Mode Delay Effects

Recall several obvious properties of lossless, terminated transmission-line systems: power conservation, passivity (no active sources), and passively realizable immittances. Mathematically, their MTL functions are constrained by

$$V(z) = V\left(z - i\frac{\lambda}{2}\right), \qquad z < 0; \quad i = 1, 2, 3, \ldots \tag{15a}$$

$$P(z) = P_L \tag{15b}$$

$$\frac{\partial}{\partial z}|\Gamma| = 0 \tag{15c}$$

$$\Re\mathrm{e}\{Z, Y\} \geq 0. \tag{15d}$$

However, in MTL systems, the immittance matrix behavior is considerably more complicated. This section illustrates that conditions (15) do not generally apply to the MTL function (conductor-domain) analogues.

A. Signal Distortion

Longitudinal mode voltage is the superposition of the forward and backward moded voltages; the mode voltage in (2a) may be combined with (9) and expressed as

$$\begin{aligned} \boldsymbol{v}_m(z) &= \boldsymbol{Q}(-z) \cdot \boldsymbol{v}^+_m + \boldsymbol{Q}(z) \cdot \boldsymbol{\Gamma}^m_L \cdot \boldsymbol{Q}(z) \cdot \boldsymbol{Q}(-z) \cdot \boldsymbol{v}^+_m \\ &= [\mathbf{1}_n + \boldsymbol{\Gamma}^m_{\rm in}(z)] \cdot \boldsymbol{Q}(-z) \cdot \boldsymbol{v}^+_m \end{aligned} \tag{16}$$

where modal decoupling results in constant modal voltage standing-wave ratios (SWRs) along the line.

Mode voltage i from (16) is given by

$$\boldsymbol{v}_m(z)]_i = [\boldsymbol{Q}(-z)]_{ii}\, \boldsymbol{v}^+_m]_i \left(1 + \frac{\boldsymbol{Q}(2z) \boldsymbol{\Gamma}^m_L \boldsymbol{v}^+_m]_i}{\boldsymbol{v}^+_m]_i} \right) \tag{17}$$

the SWR of the ith mode is, therefore [15],

$$\mathrm{SWR}_m]_i = \frac{1 + \left| \dfrac{\boldsymbol{\Gamma}^m_L \boldsymbol{v}^+_m]_i}{\boldsymbol{v}^+_m]_i} \right|}{1 - \left| \dfrac{\boldsymbol{\Gamma}^m_L \boldsymbol{v}^+_m]_i}{\boldsymbol{v}^+_m]_i} \right|}. \tag{18}$$

Clearly, (18) confirms the constant longitudinal magnitudes of the modal reflection coefficient for lossless coupled lines. The terms $\boldsymbol{\Gamma}^m_L \boldsymbol{v}^+_m]_i / \boldsymbol{v}^+_m]_i$ in (17) and (18) indicate the general dependence of the ith mode on all n forward voltage coefficients at the load $\boldsymbol{v}^+_m$ and the ith row of $\boldsymbol{\Gamma}^m_L$. This dependency is a physical result of mode conversion at a discontinuity. A significant consequence of this dependence is that a purely real (resistive) load termination network will not necessarily result in a modal standing wave minimum or maximum at $z = 0$ for a system with mode delays.

It is evident from (17) that the longitudinal conductor voltages and currents have nonuniform SWRs since each is a linear combination (1) of all mode voltages or currents, respectively. Therefore, a definition of conductor SWR_c along lossless coupled lines would only apply to successive maxima and minima.

MTL power may be quantified in either the mode or conductor domain for microstrip [7, eqs. (53) and (55)]. Excitations are represented in Thevenin form with a conductor voltage

source vector $\boldsymbol{v}_S$ and source impedance network matrix $\boldsymbol{\mathcal{Z}}_S^c$. The total power traveling down a lossless line is a constant equal to the power dissipated in the arbitrary passive load

$$P_L = P(z) = \frac{1}{2}\Re\mathrm{e}\{\boldsymbol{v}^*(z)\cdot\boldsymbol{i}(z)\} \tag{19a}$$

$$= \frac{1}{2}\Re\mathrm{e}\{\boldsymbol{v}_m^*(z)\cdot\boldsymbol{i}_m(z)\} \tag{19b}$$

where $(^*)$ denotes "complex conjugate transpose."

If (19b) is expressed as the sum of forward and backward powers, we find that individual mode powers are constants in z. However, expanding (19a) into the sum of n terms as functions of the mode voltages, eigenvectors, and propagators reveals the conductor power fluctuations along the longitudinal direction—a result quite different from the single transmission-line case (15b).

The total power is the sum of the powers incident on each conductor or the sum of the n modal powers. Despite the individual conductor power variations along z, the sum of n conductor powers is always P_L.

B. Longitudinal Power Conservation

Now, we consider the features of the longitudinal reflection coefficient matrix functions. In lossless coupled-line systems without mode delay, the magnitude of the modal reflection coefficient elements $[\boldsymbol{\Gamma}_{\mathrm{in}}^c(z)]_{ij}$ remain constant along z, and their phase is linear within each period. This fact is consistent with the power orthogonality of the quasi-TEM modes, and will be clearly demonstrated via numerical simulations in Section IV. With mode delays, however, (10) shows that each term of $\boldsymbol{\Gamma}_{\mathrm{in}}^c(z)$ is a linear combination of n^2 distinct z-varying phasors, which include *all* propagation constants γ_i. Therefore, the magnitudes of matrix terms $[\boldsymbol{\Gamma}_{\mathrm{in}}^c(z)]_{ij}$ clearly vary with z.

For lossless lines with symmetric $\boldsymbol{Y}_L^c$, $\boldsymbol{\Gamma}_L^m$ and $\boldsymbol{\Gamma}_{\mathrm{in}}^m(z)$ are "checkered" with zeros; in this case, each term in $\boldsymbol{\Gamma}_{\mathrm{in}}^c(z)$ contains the sum of $1/4\left[n^2+2n+(n \bmod 2)\right]$ distinct constant magnitude phasors containing separate even- and odd-mode additive combinations of γ_i: $2\gamma_1, \gamma_1+\gamma_3, \gamma_1+\gamma_5, \ldots, 2\gamma_2, \gamma_2+\gamma_4, \ldots$.

Does the longitudinal magnitude variation of $[\boldsymbol{\Gamma}_{\mathrm{in}}^c(z)]_{ij}$ violate conservation of power flowing longitudinally? From physical intuition, lossless passive lines should neither dissipate, nor generate power, therefore, longitudinal power should be conserved. The propagation constants for lossless lines are purely imaginary, thus

$$|\det[\boldsymbol{Q}(z)]| = 1. \tag{20}$$

Since the remaining matrices in (10) are constant (with respect to z), the relationship $\det(\boldsymbol{AB},\ldots,\boldsymbol{C}) = \det(\boldsymbol{A})\cdot\det(\boldsymbol{B})\cdot\cdots\cdot\det(\boldsymbol{C})$ confirms that

$$\frac{\partial}{\partial z}\left(\left|\det\left[\boldsymbol{\Gamma}_{\mathrm{in}}^c(z)\right]\right|\right) = 0 \tag{21}$$

clearly maintains a constant determinant over z. This result is physically intuitive for lossless lines: no power should be gained or lost in the longitudinal direction. Note that this result does not prove power conservation for the overall system of lines and terminations.

For practical applications, close proximity $(z < \lambda/2)$ between the matching networks and the load is often desired. In this region of small coupling length, $\boldsymbol{\Gamma}_{\mathrm{in}}^c(z)$ terms maintain approximately constant magnitude. However, with increasing length or coupling, a mixed-mode signal suffers distortion. It remains as future work to determine conditions when signal distortion due to mode delay dominates the dispersion encountered in a lossy dielectric system.

C. Passivity of the Admittance Matrix

The mode delays [and the behavior of (10)] also manifest themselves in another interesting effect. Suppose we realize $\boldsymbol{Y}_{\mathrm{in}}^c(z)$ as a passive N-terminal circuit network, given by $\boldsymbol{\mathcal{Z}}_{\mathrm{in}}(z)$. Given arbitrary passive terminations, the mode delays may yield $\boldsymbol{Y}_{\mathrm{in}}^c(z)$, whose off-diagonal elements contain positive real parts, i.e.,

$$\Re\left\{[\boldsymbol{\mathcal{Z}}_{\mathrm{in}}(z)]_{ij}, [\boldsymbol{\mathcal{Y}}_{\mathrm{in}}(z)]_{ij}\right\} < 0, \qquad i \neq j \tag{22}$$

which at first appears to violate passivity.

Condition (22) appears to be a consequence of the conductor reflection coefficient magnitude variations; indeed, (22) can be mathematically justified in a two-line case given large magnitude fluctuations in $\boldsymbol{\Gamma}_{\mathrm{in}}^c(z)$, which are clearly conceivable (with simulation results presented in Section III-D). For $n \geq 3$, the analysis grows considerably more complicated, and numerical evaluations become necessary. However, in typical systems, (22) may be satisfied at many longitudinal points, as will be demonstrated in Section IV.

Despite this superficially problematic result, there is no physical reason to suspect that the input admittance matrix $\boldsymbol{Y}_{\mathrm{in}}^c(z)$ represents a nonpassive network. As an n-dimensional driving-point short-circuit admittance matrix, a realization of $\boldsymbol{Y}_{\mathrm{in}}^c(z=-a)$ would model the length a of lines and their prescribed termination at $z=0$. This realized network is passive if the total average signal power entering all the ports is greater than or equal to zero. We may easily verify this passivity by generalizing the derivation in [18] for power entering n ports as follows:

$$P = \boldsymbol{v}_c(z)^* \cdot \left(\Re\mathrm{e}\left\{\boldsymbol{Y}_{\mathrm{in}}^c(z)\right\}\right)\cdot\boldsymbol{v}_c(z). \tag{23}$$

Therefore, the passivity of $\boldsymbol{Y}_{\mathrm{in}}^c(z)$ may be easily verified by checking if the immittance function $\Re\{\boldsymbol{Y}_{\mathrm{in}}^c(z)\}$ is positive definite. Simulation results for the three-line case will be shown in Section III-D.

D. Realizability of the Admittance Matrix

While we can justify (22) algebraically via a simple two-line case and check the passivity of $\boldsymbol{Y}_{\mathrm{in}}^c(z)$ via (23), we should also consider passive N-terminal circuit realization (e.g., Fig. 1) of $\boldsymbol{Y}_{\mathrm{in}}^c(z)$ for all z. In other words, what are the topological realizability conditions of matrix $\boldsymbol{Y}_{\mathrm{in}}^c(z)$?

In lossless lines, the distributed admittance matrix and propagation constants are purely imaginary. The distributed capacitance matrix $\boldsymbol{C}$ is a dominant matrix [19], which renders the characteristic impedance and admittance matrices real and dominant by virtue of (4). In network synthesis, an $(n\times n)$ dominant real admittance matrix may be realized as a resistive/conductive

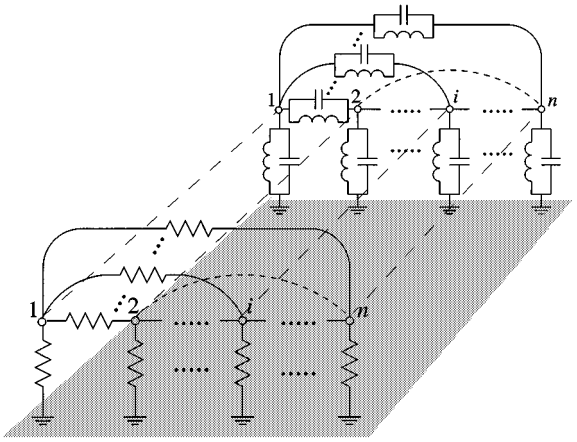

Fig. 3. Parallel conductance and susceptance circuits composing an N-node n-terminal impedance network with a common ground.

network consisting of, in general, $2n$ nodes [20]. Furthermore, if all off-diagonal terms of this matrix are nonpositive, then a resistive/conductive network of N terminals may be synthesized [20, Th. 8-4] with the real parts of the impedance/admittance network matrices (13).

However, $\boldsymbol{Y}_{\text{in}}^{c}(z)$ is generally a complex matrix. Therefore, Theorem 8-4 must be extended accordingly. We split the N-terminal realization of $\boldsymbol{Y}_{\text{in}}^{c}(z)$ into a conductive network in parallel with a susceptive network (both N-terminal, using the real and imaginary parts, respectively) as shown in Fig. 3. Then, since the susceptance network is realized with inductors or capacitors, the sign constraints apply only to the real parts of the admittance matrix or the conductive network. Thus, the theorem applies to (complex) admittance matrices.

The equivalent network topology is an N-node polygon interconnected with impedances as per $\boldsymbol{\mathcal{Z}}_{\text{in}}$. These impedances are realized as parallel *RL* or *RC* circuits where

$$R_{ij}(z) = \left(\Re\mathrm{e}\{[\boldsymbol{\mathcal{Y}}_{\text{in}}(z)]_{ij}\}\right)^{-1} \tag{24a}$$

$$L_{ij}(z) = \frac{\left(\Im\mathrm{e}\{[\boldsymbol{\mathcal{Y}}_{\text{in}}(z)]_{ij}\}\right)^{-1}}{\omega}, \qquad \Im\mathrm{e}\{[\boldsymbol{\mathcal{Y}}_{\text{in}}]_{ij}\} < 0 \tag{24b}$$

$$C_{ij}(z) = \omega\left(\Im\mathrm{e}\{[\boldsymbol{\mathcal{Y}}_{\text{in}}(z)]_{ij}\}\right)^{-1}, \qquad \Im\mathrm{e}\{[\boldsymbol{\mathcal{Y}}_{\text{in}}]_{ij}\} > 0. \tag{24c}$$

Now, if all off-diagonal terms of the dominant matrix $\boldsymbol{Y}_{\text{in}}^{c}(z)$ in microstrip have nonpositive real parts, $\boldsymbol{Y}_{\text{in}}^{c}(z)$ is passively realized as an N-terminal *RLC* circuit network (as in Fig. 1). This realization assumes the topology of a complete polygon with N vertices and $N(N-1)/2$ admittances, $1/4\left[n^2+2n+(n \bmod 2)\right]$ of which are independent (see Fig. 1), and whose components are given by (24).

However, a dominant admittance matrix $\boldsymbol{Y}_{\text{in}}^{c}(z=-a)$ whose off-diagonal terms have positive real components (22) is realizable as an n-port *RLC* network that has only N nodes, but no common ground for all ports (the general synthesis procedure may be found in [20]). In this case, it follows that $\boldsymbol{Y}_{\text{in}}^{c}(-a)$ is unrealizable at $z=-a$ as an N-terminal *RLC* circuit network since coupled microstrip network topology does have a common ground. An alternative realization consisting of $2n$ nodes and n ports exists, though it lacks a common ground. Of course, this $2n$-node realization also applies when $\boldsymbol{Y}_{\text{in}}^{c}(-a)$ has all off-diagonal real components nonpositive since its N-terminal network realization may also take the form of $2n$-node, n-port realization with no common ground, where both realizations are interchangeable via star-mesh conversions.

However, how is such a topology without a common ground reconciled with the physics of microstrip? Furthermore, how can the section of lines length a and their termination be passively realized? We must consider another circuit element: the ideal transformer. If permitted in the equivalent *RLC* circuit realization of $\boldsymbol{Y}_{\text{in}}^{c}(-a)$, one node may be designated as the common ground and the remaining ports may be isolated by these transformers and then connected to the same common ground. Therefore, at points where (22) is encountered, the application of ideal transformers to $n-1$ ports of the $2n$-node realization without a common ground will permit n-port, N-node common-ground realization. This possibility arises since any synthesis procedure for realizing an n-port network with ideal transformers simultaneously realizes an N-terminal network [20].

Hence, we have shown that (22) for certain longitudinal points $z=-a$ does not violate passivity of the terminated system, thus numerical stability at $z=-a$ is preserved, and will be illustrated in Section IV. However, a passive unbalanced N-node n-port *RLC* termination network with one common ground (the microstrip ground plane) is not realizable at $z=-a$ without transformers.

Expounding the physical meaning of the ideal transformers, they dissipate no real power and store no energy. Moreover, if the turn ratios are 1 : 1, their only function is to isolate a port and allow for common grounding and the realization of an N-terminal topology. Of course, they only become necessary when (22) is encountered. Arguably the most significant effect of the mode delays is the longitudinal power fluctuations along the conductors, which depend on the conductor voltage and current magnitude variations, and these effectively require compensation in the immittance parameters. Condition (22) provides this compensation, though not in a readily discernible manner.

IV. Numerical Results

Numerical results presented in this section have previously appeared in the literature [8], though more longitudinal details are presented. A three-coupled line microstrip structure with circuit parameters $\boldsymbol{R}=\boldsymbol{0}$, $\boldsymbol{G}=\boldsymbol{0}$, and

$$\boldsymbol{L} = \begin{bmatrix} 310.887 & 67.4845 & 22.2536 \\ 67.4845 & 305.963 & 67.4845 \\ 22.2536 & 67.4845 & 310.887 \end{bmatrix} \text{ nH} \tag{25}$$

$$\boldsymbol{C} = \begin{bmatrix} 125.143 & -15.4225 & -0.81741 \\ -15.4225 & 128.346 & -15.4225 \\ -0.81741 & -15.4225 & 125.143 \end{bmatrix} \text{ pF} \tag{26}$$

was synthesized on board for a three-coupled-line matching network. Moderate coupling ensured discernible mode delays for an operating frequency of 2.0 GHz. A "low impedance" termination at the load given by

$$\boldsymbol{\mathcal{Z}}_{L} = \begin{bmatrix} 20 & 287.152 & 2883.71 \\ 287.152 & 69.1719 & 287.152 \\ 2883.71 & 287.152 & 20 \end{bmatrix} \Omega \tag{27}$$

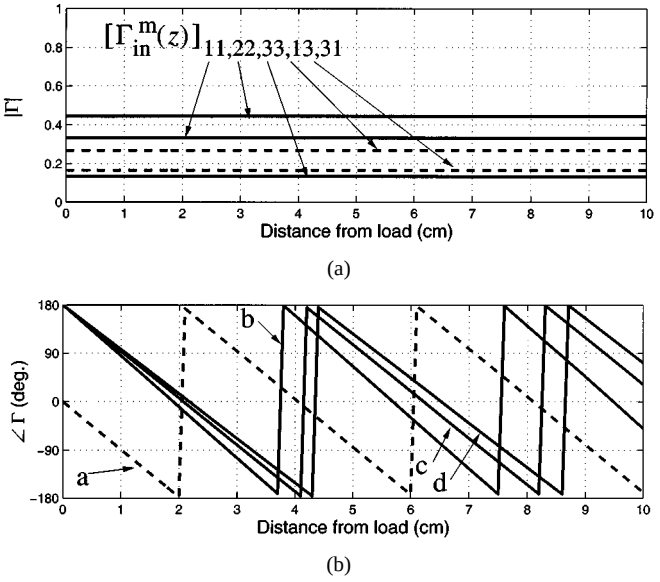

Fig. 4. Longitudinal variations of the input modal reflection coefficient matrix terms. Note: $a = [\mathbf{\Gamma}_{\rm in}^{m}(z)]_{13,31}$, $b = [\mathbf{\Gamma}_{\rm in}^{m}(z)]_{11}$, $c = [\mathbf{\Gamma}_{\rm in}^{m}(z)]_{22}$, and $d = [\mathbf{\Gamma}_{\rm in}^{m}(z)]_{33}$.

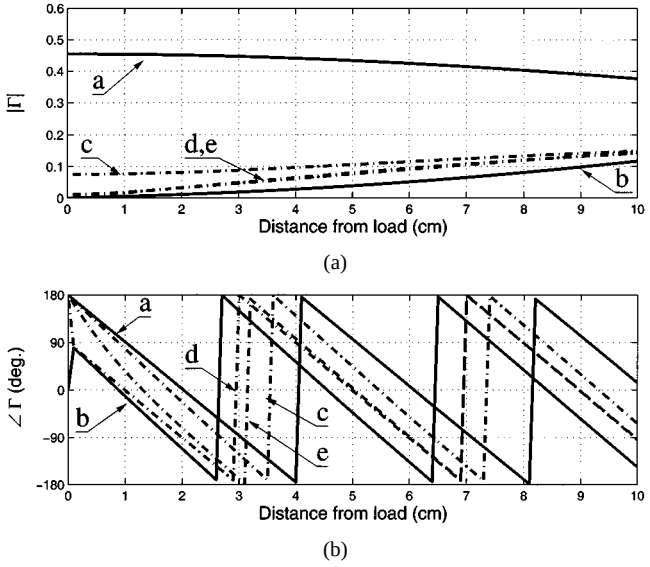

Fig. 5. Longitudinal variations of the input conductor reflection coefficient matrix $\mathbf{\Gamma}_{\rm in}^{c}(z)$ terms. Note: $a = [\mathbf{\Gamma}_{\rm in}^{c}(z)]_{11,33}$, $b = [\mathbf{\Gamma}_{\rm in}^{c}(z)]_{22}$, $c = [\mathbf{\Gamma}_{\rm in}^{c}(z)]_{21,23}$, $d = [\mathbf{\Gamma}_{\rm in}^{c}(z)]_{12,32}$, and $e = [\mathbf{\Gamma}_{\rm in}^{c}(z)]_{13,31}$.

and an excitation of 1 V with a 50-Ω source impedance on each line resulted in multimode reflections simulated via an MTL digital computer program.

As predicted in Section III-B, the elements of $\mathbf{\Gamma}_{\rm in}^{m}(z)$ maintain constant longitudinal magnitudes; all five nonzero elements are shown in Fig. 4. Three distinct phase constants (and the arithmetic mean of modes 1 and 3) are readily apparent in the phase plot. Also evident is the 180° phase at $z = 0$ due to the low-impedance termination.

Clearly, for lossless systems, terms in $\mathbf{\Gamma}_{\rm in}^{c}(z)$ exhibit nonlinear magnitude dependence with z. Matrix $\mathbf{\Gamma}_{\rm in}^{c}(z)$ terms are shown in Fig. 5. Within practical working distance from the terminations ($z > -10$ cm), the magnitude of the all voltage reflection terms increase with the coupling length, except for the self reflection terms $[\mathbf{\Gamma}_{\rm in}^{c}(z)]_{11,33}$, which steadily decrease. For moderate to low coupling or short distances from the terminations, the impact from these effects is obviously minimum.

To better exemplify the properties of longitudinal mode and conductor voltage magnitudes in lossless lines, a large length $D = 50$ cm was simulated. The standing-wave patterns are shown in Fig. 6. As predicted, each mode voltage standing-wave pattern is characterized by a minima offset from the load and a distinct constant SWR. At large distances, a phase offset between the standing-wave patterns becomes apparent. The resulting shift in the conductor voltage signals is shown in Fig. 6. Clearly, as predicted analytically, the mode SWRs remain constant, and have periods of $z = \beta_i/2$. Conductor voltage standing-wave patterns neither have a fixed maximum-minimum ratio, nor simply quantifiable periods.

Power behaves similarly; constant longitudinal mode powers are observed in Fig. 7, while the conductor power fluctuations (the slowly varying envelope) due to the mode delays are evident. The negative power for mode 3 suggests that power is generated at the load and questions passivity. However, this is simply mode conversion: a fraction of power from mode 1 is converted to mode 3, whose reflected magnitude exceeds its incident magnitude. Note that the sum of the three conductor

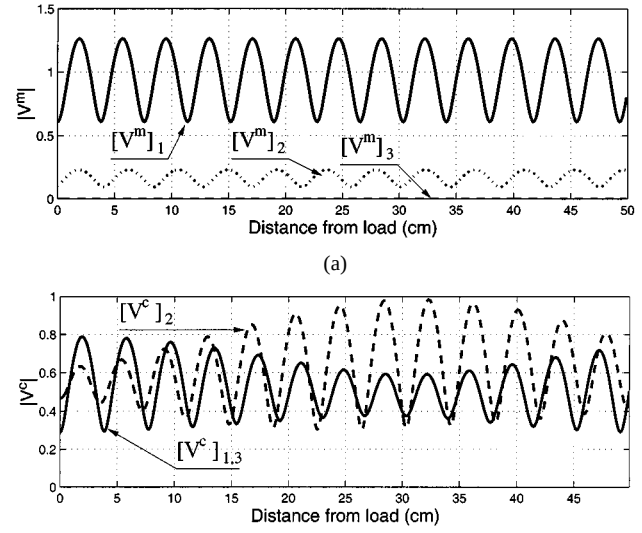

Fig. 6. Simulated longitudinal variation (from load to $z = -50$ cm) of modal and conductor voltage magnitudes for "short" termination at 2.0 GHz, showing the magnitude properties for lossless lines.

powers is constant for all z and equal to the sum of the mode powers.

Finally, the longitudinal input admittance matrix function is plotted to illustrate an "active" effect (22). Matrix $\boldsymbol{Y}_{\rm in}^{c}(z)$ is normalized via elements to illustrate specific locations where (22) holds as follows:

$$
\begin{aligned}
Y_{\rm self}(z) &= \frac{[\mathcal{Y}_{\rm in}^{c}(z)]_{11}}{[\mathcal{Y}_{\rm ch}^{c}]_{11}} \\
Y_{\rm self-2}(z) &= \frac{[\mathcal{Y}_{\rm in}^{c}(z)]_{22}}{[\mathcal{Y}_{\rm ch}^{c}]_{22}} \\
Y_{\rm mut}(z) &= \frac{[\mathcal{Y}_{\rm in}^{c}(z)]_{12}}{[\mathcal{Y}_{\rm ch}^{c}]_{12}} \\
Y_{\rm non}(z) &= \frac{[\mathcal{Y}_{\rm in}^{c}(z)]_{13}}{[\mathcal{Y}_{\rm ch}^{c}]_{13}}
\end{aligned}
\tag{28}
$$

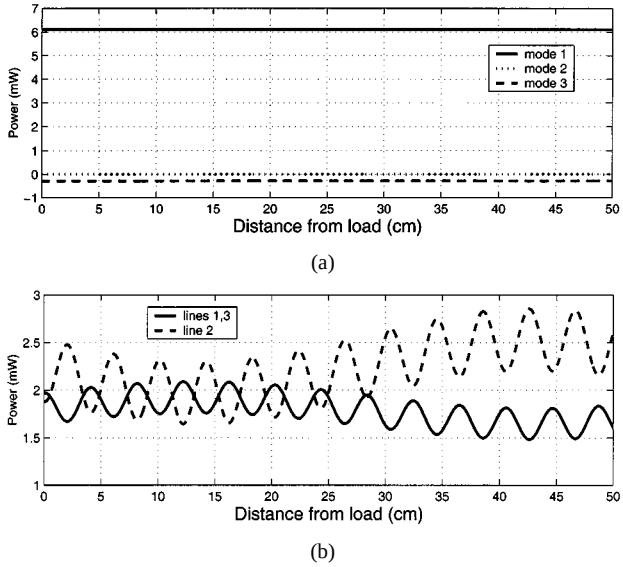

Fig. 7. Longitudinal distribution of the conductor and modal powers (from load to $z = -50$ cm).

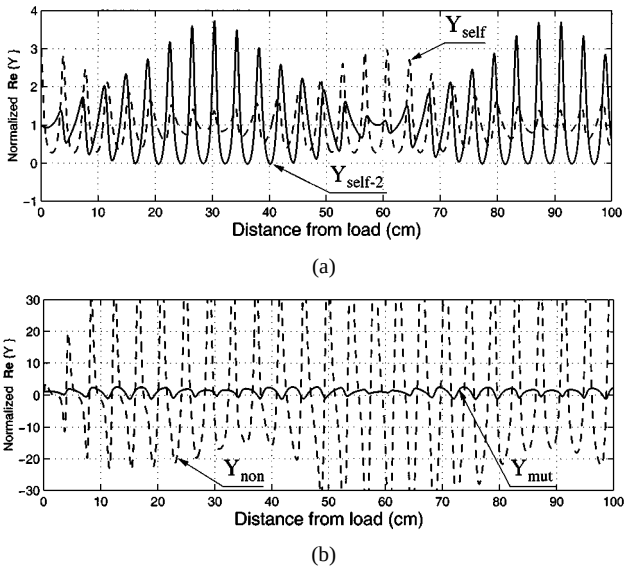

Fig. 8. Simulated longitudinal variation (from load to $z = -100$ cm) of $\Re\{\boldsymbol{Y}^c_{\rm in}(z)\}$ for "short" termination at 2.0 GHz, showing the negative real components of the element-normalized admittance matrix.

where $Y_{\rm self}$ connects lines 1 and 3 to ground, $Y_{\rm self-2}$ connects line 2 to ground, $Y_{\rm mut}$ is the mutual admittance between nearest neighbors, and $Y_{\rm non}$ is the admittance between nonadjacent neighbors (lines 1 and 3).

Fig. 8 shows locations for which each of these admittances have negative real parts, and are unrealizable in an N-terminal topology. Clearly, the periodicity of the effect is evident. A detailed evaluation of how the termination choice affects this longitudinal occurrence is a highly nonlinear problem beyond the scope of this paper.

For great lengths, we find locations where $\boldsymbol{Y}^c_{\rm in}(z)$ is not dominant shown *a posteriori*. However, in these instances, none of the diagonal terms of $[\boldsymbol{Y}^c_{\rm in}(z)]_{ii}$ have negative real parts. As expected, the admittance matrix was positive real (therefore, passive) for all simulated points, demonstrating numerical stability and correct longitudinal MTL formulations. In regards to the realizability of $\boldsymbol{Y}^c_{\rm in}(z)$, the condition of dominance is sufficient, but not necessary; the only constraint on passive realization (with *RLC* elements, ideal transformers, and mutual inductance) is that $\boldsymbol{Y}^c_{\rm in}(z)$ is positive real [20, Th. 7-2]. Indeed, the function $\boldsymbol{Y}^c_{\rm in}(z)$ could be realized everywhere with a common-ground topology including transformers.

V. Conclusions

The objective of this paper has been to investigate the behavior of the longitudinal MTL functions and, in particular, detail the effects of quasi-TEM mode delays on these functions. This study has showed how the mode delays in lossless symmetric lines were responsible for longitudinal conductor power variations, varying conductor voltage SWRs, multimode signal distortion, conductor reflection coefficient magnitude variations, and unrealizable N-terminal admittance matrices.

Passivity, reciprocity, and lossless properties have been demonstrated numerically for the cases encountered, and passive circuit realizations have always been possible, though constrained to certain topologies; the N-terminal topology physically inherent to microstrip could have been realized in the general case only if ideal transformers had been included.

For the lossy case, such analysis becomes considerably more complicated, though the present analysis should be useful for many circuits of practical interest modeled using lossless assumptions. Moreover, as designers simulate smaller, faster, and higher frequency transmission devices, particularly coupled transmission lines, these effects will become more pronounced. Clearly, lossy high-coupling MTL simulation must account for these effects to ensure that large longitudinal reflection coefficient magnitude fluctuations, conductor power variations, and signal distortion are not attributed solely to power loss or other mechanisms.

Detailed analysis regarding the effects of mode delays on loss calculation, as well as experimental validation on low-loss structures, remains as a topic of future work.

Appendix

S-parameter matrix symmetry in reciprocal systems is shown as follows (omitting the matrix multiplication operator $\cdot$).

The generalized S-parameter matrix given by (14) is repeated here for convenience as follows:

$$\boldsymbol{S} = (\boldsymbol{Z}^c_{\rm ch})^{1/2}\,[\boldsymbol{Z}^c_{\rm ch} + \boldsymbol{Z}^c_L]^{-1}\,[\boldsymbol{Z}^c_L - \boldsymbol{Z}^c_{\rm ch}]\,(\boldsymbol{Z}^c_{\rm ch})^{-1/2}. \quad \text{(A1)}$$

This matrix describes a reciprocal system; its symmetry is proven as follows. Taking the transpose of (A1) results in

$$\boldsymbol{S}^t = (\boldsymbol{Z}^c_{\rm ch})^{-1/2}\,[\boldsymbol{Z}^c_L - \boldsymbol{Z}^c_{\rm ch}]\,[\boldsymbol{Z}^c_{\rm ch} + \boldsymbol{Z}^c_L]^{-1}\,(\boldsymbol{Z}^c_{\rm ch})^{1/2} \quad \text{(A2)}$$

where each factor is symmetric by reciprocity. Now, if $\boldsymbol{Z}^c_{\rm ch}$ is nonsingular

$$\boldsymbol{S}^t = (\boldsymbol{Z}^c_{\rm ch})^{-1/2}\,\boldsymbol{Z}^c_{\rm ch}\,(\boldsymbol{Z}^c_{\rm ch})^{-1}\,[\boldsymbol{Z}^c_L - \boldsymbol{Z}^c_{\rm ch}] \cdot [\boldsymbol{Z}^c_{\rm ch} + \boldsymbol{Z}^c_L]^{-1}\,\boldsymbol{Z}^c_{\rm ch}\,(\boldsymbol{Z}^c_{\rm ch})^{-1}\,(\boldsymbol{Z}^c_{\rm ch})^{1/2}. \quad \text{(A3)}$$

To simplify the algebra, we let

$$\boldsymbol{A} = (\boldsymbol{Z}^c_{\rm ch})^{-1}\,[\boldsymbol{Z}^c_L - \boldsymbol{Z}^c_{\rm ch}]\,[\boldsymbol{Z}^c_{\rm ch} + \boldsymbol{Z}^c_L]^{-1}\,\boldsymbol{Z}^c_{\rm ch}. \quad \text{(A4)}$$

Note that $\boldsymbol{A}$ is similar to a reflection coefficient. Now,

$$\begin{aligned}\boldsymbol{A} &= (\boldsymbol{Z}^c_{\rm ch})^{-1}\,\boldsymbol{Z}^c_L\,[\boldsymbol{Z}^c_{\rm ch}+\boldsymbol{Z}^c_L]^{-1}\,\boldsymbol{Z}^c_{\rm ch} - [\boldsymbol{Z}^c_{\rm ch}+\boldsymbol{Z}^c_L]^{-1}\,\boldsymbol{Z}^c_{\rm ch}\\ &= \left\{(\boldsymbol{Z}^c_{\rm ch})^{-1}\,[\boldsymbol{Z}^c_{\rm ch}+\boldsymbol{Z}^c_L]\,(\boldsymbol{Z}^c_L)^{-1}\,\boldsymbol{Z}^c_{\rm ch}\right\}^{-1}\\ &\quad - [\boldsymbol{Z}^c_{\rm ch}+\boldsymbol{Z}^c_L]^{-1}\,\boldsymbol{Z}^c_{\rm ch}\\ &= \left\{\mathbf{1}_n + (\boldsymbol{Z}^c_L)^{-1}\,\boldsymbol{Z}^c_{\rm ch}\right\}^{-1} - [\boldsymbol{Z}^c_{\rm ch}+\boldsymbol{Z}^c_L]^{-1}\,\boldsymbol{Z}^c_{\rm ch}\\ &= \left\{(\boldsymbol{Z}^c_L)^{-1}\,[\boldsymbol{Z}^c_{\rm ch}+\boldsymbol{Z}^c_L]\right\}^{-1} - [\boldsymbol{Z}^c_{\rm ch}+\boldsymbol{Z}^c_L]^{-1}\,\boldsymbol{Z}^c_{\rm ch}\\ &= [\boldsymbol{Z}^c_L+\boldsymbol{Z}^c_{\rm ch}]^{-1}\,[\boldsymbol{Z}^c_L-\boldsymbol{Z}^c_{\rm ch}]. \end{aligned} \tag{A5}$$

The derivation for $\boldsymbol{A}$ is obviously applicable to (6).

Using (A5) with (A4) and (A3), we arrive at

$$\begin{aligned}\boldsymbol{S}^t &= (\boldsymbol{Z}^c_{\rm ch})^{1/2}\,\boldsymbol{A}\,(\boldsymbol{Z}^c_{\rm ch})^{-1/2}\\ &= (\boldsymbol{Z}^c_{\rm ch})^{1/2}\,[\boldsymbol{Z}^c_L+\boldsymbol{Z}^c_{\rm ch}]^{-1}\,[\boldsymbol{Z}^c_L-\boldsymbol{Z}^c_{\rm ch}]\,(\boldsymbol{Z}^c_{\rm ch})^{-1/2}. \end{aligned} \tag{A-6}$$

Finally, we have $\boldsymbol{S}=\boldsymbol{S}^t$, which agrees with [21], in which Chin defines $\boldsymbol{S}$ according to (A2).

ACKNOWLEDGMENT

The authors wish to acknowledge V. Okhmatovski, Department of Electrical and Computer Engineering, University of Illinois at Urbana-Champaign (UIUC), M. Kowalski, Department of Electrical and Computer Engineering, UIUC, V. Kawadia, Department of Electrical and Computer Engineering, UIUC, and H.-Y. Chung, Department of Electrical and Computer Engineering, UIUC, for helpful review and presentation suggestions.

REFERENCES

[1] D. Kajfez, "Multiconductor transmission lines," Master's thesis, Dept. Elect. Eng., Univ. Mississippi, Mississippi, MS, 1972.
[2] K. D. Marx, "Propagation modes, equivalent circuits, and characteristic terminations for multiconductor transmission lines with inhomogeneous dielectrics," *IEEE Trans. Microwave Theory Tech.*, vol. MTT-21, pp. 450–457, July 1973.
[3] C. R. Paul, "On uniform multimode transmission lines," *IEEE Trans. Microwave Theory Tech.*, vol. MTT-21, pp. 556–558, Aug. 1973.
[4] D. F. Williams, L. A. Hayden, and R. B. Marks, "A complete multimode equivalent-circuit theory for electrical design," *J. Res. Natl. Stand. Technol.*, vol. 102, pp. 405–423, Jul.–Aug. 1997.
[5] T. R. Arabi, T. K. Sarkar, and A. R. Djordjevic, "Time and frequency domain characterization of multiconductor transmission lines," *Electromagnetics*, vol. 9, pp. 85–112, 1989.
[6] V. K. Tripathi, "On the analysis of symmetrical three-line microstrip circuits," *IEEE Trans. Microwave Theory Tech.*, vol. MTT-25, pp. 726–729, Sept. 1977.
[7] C. R. Paul, "Decoupling the multiconductor transmission line equations," *IEEE Trans. Microwave Theory Tech.*, vol. 44, pp. 1429–1440, Aug. 1996.
[8] J. G. Nickel and J. E. Schutt-Aine, "Several narrowband matching networks for quasi-TEM coupled microstrip lines," in *IEEE 9th Topical Elect. Performance Electron. Packag. Meeting*, Oct. 2000, pp. 296–299.
[9] Y.-Y. Sun, "Immittance matrices of multiconductor transmission lines," *J. Franklin Inst.*, vol. 307, pp. 59–67, Jan. 1979.
[10] ——, "Matrix theorems of multiconductor transmission lines," *J. Chinese Inst. Eng.*, vol. 1, pp. 37–41, Sept. 1978.
[11] T. Cholewicki, "Some properties of immittance matrices of a nonuniform n-wire transmission line," *Bull. Acad. Pol. Sci. Ser. Sci. Tech.*, vol. 30, pp. 101–107, 1982.
[12] L. Carin and K. J. Webb, "Characteristic impedance of multilevel, multiconductor hybrid mode microstrip," *IEEE Trans. Magn.*, vol. 25, pp. 2947–2949, July 1989.
[13] J. E. Schutt-Aine and R. Mittra, "Nonlinear transient analysis of coupled transmission lines," *IEEE Circuits Syst. I*, vol. 36, pp. 959–966, July 1989.
[14] ——, "Analysis of pulse propagation in coupled transmission lines," *IEEE Circuits Syst. I*, vol. CAS-32, pp. 1214–1219, Dec. 1985.
[15] J. G. Nickel, "Synthesis of several narrow-band matching networks for quasi-TEM coupled microstrip lines with passive terminations," Master's thesis, Dept. Comput. Elect. Eng., Univ. Illinois at Urbana-Champaign, Urbana-Champaign, IL, 1999.
[16] J. T. Kuo and C. H. Tzuang, "A termination scheme for high-speed pulse propagation on a system of tightly coupled coplanar strips," *IEEE Trans. Microwave Theory Tech.*, vol. 42, pp. 1008–1015, June 1994.
[17] S. Amari and J. Bornemann, "Optimum termination networks for tightly coupled microstrip lines under random and deterministic excitations," *IEEE Trans. Microwave Theory Tech.*, vol. 45, pp. 1785–1789, Oct. 1997.
[18] R. Carson, *High-Frequency Amplifiers*. New York: Wiley, 1982.
[19] R. M. Fano, L. J. Chu, and R. B. Adler, *Electromagnetic Fields, Energy, and Forces*. New York: Wiley, 1960.
[20] L. Weinberg, *Network Analysis and Synthesis*. New York: McGraw-Hill, 1962.
[21] Y. K. Chin, "Analysis and applications of multiple coupled line structures in an inhomogeneous medium," Ph.D. dissertation, Dept. Elect. Comput. Eng., Oregon State Univ., Corvallis, OR, 1982.

Josh G. Nickel (S'95) was born on November 27, 1974, in Lancaster, PA. He received the B.S. degree (with honors) in electrical engineering from the Pennsylvania State University, University Park, in 1997, and the M.S. and Ph.D. degrees in electrical engineering from the University of Illinois at Urbana-Champaign, in 1999 and 2001, respectively.

As a graduate student, he held a research assistantship at the Center for Computational Electromagnetics, University of Illinois at Urbana-Champaign, from 1997 to 2001, and was a Teaching Assistant in automated microwave measurements for six semesters. He assisted in the construction of a 16-processor parallel Linux cluster or "Beowulf" supercomputer. He has held internships at AMP Inc., the MITRE Corporation, IBM, and SAIC/Demaco. He is currently with Silicon Bandwidth Inc., Fremont, CA. His current research interests are in opto-electronic packaging, high-speed connectors, and multiconductor transmission-line simulation and analysis.

José E. Schutt-Ainé (S'86–M'86–SM'98) received the B.S. degree from the Massachusetts Institute of Technology (MIT), Cambridge, in 1981, and M.S. and Ph.D. degrees from the University of Illinois at Urbana-Champaign (UIUC), in 1984 and 1988, respectively.

From 1981 to 1983, he was an Application Engineer at the Hewlett-Packard Microwave Technology Center, Santa Rosa, CA, where he was involved with transistor modeling. He held summer positions at GTE Network Systems, Northlake, IL. In 1989, he joined the faculty of the Electromagnetic Communication Laboratory, UIUC, where he is currently an Associate Professor of electrical and computer engineering. His research interests include microwave theory and measurements, electromagnetics, high-frequency circuit design, and electronic packaging.